

The remnants of galaxy formation from a panoramic survey of the region around M31

Alan W. McConnachie¹, Michael J. Irwin², Rodrigo A. Ibata³, John Dubinski⁴, Lawrence M. Widrow⁵, Nicolas F. Martin⁶, Patrick Côte¹, Aaron L. Dotter⁷, Julio F. Navarro⁷, Annette M. N. Ferguson⁸, Thomas H. Puzia¹, Geraint F. Lewis⁹, Arif Babul⁷, Pauline Barmby¹⁰, Olivier Bienayme³, Scott C. Chapman², Robert Cockcroft¹¹, Michelle L. M. Collins², Mark A. Fardal¹², William E. Harris¹¹, Avon Huxor¹³, A. Dougal Mackey⁸, Jorge Peñarrubia², R. Michael Rich¹⁴, Harvey B. Richer¹⁵, Arnaud Siebert³, Nial Tanvir¹⁶, David Valls-Gabaud¹⁷ & Kimberly A. Venn⁷

¹*NRC Herzberg Institute of Astrophysics, 5071 West Saanich Road, Victoria, British Columbia, Canada V9E 2E7.*

²*Institute of Astronomy, University of Cambridge, Madingley Road, Cambridge CB3 0HA, UK.*

³*Observatoire de Strasbourg, 11, rue de l'Université, F-67000 Strasbourg, France.*

⁴*Department of Astronomy & Astrophysics, University of Toronto, 50 St. George Street, Toronto, Ontario, Canada M5S 3H4.*

⁵*Department of Physics, Engineering Physics, and Astronomy Queen's University, Kingston, Ontario, Canada K7L 3N6.*

⁶*Max-Planck-Institut für Astronomie, Königstuhl 17, D-69117 Heidelberg, Germany.*

⁷*Department of Physics and Astronomy, University of Victoria, 3800 Finnerty Road, Victoria, British Columbia, Canada V8P 5C2.*

⁸*Institute for Astronomy, University of Edinburgh, Royal Observatory, Blackford Hill, Edinburgh EH9 3HJ, UK.*

⁹*Sydney Institute for Astronomy, School of Physics, University of Sydney, NSW2006, Australia.*

¹⁰*Department of Physics and Astronomy, University of Western Ontario, 1151 Richmond Street, London, Ontario, Canada N6A 3K7.*

¹¹*Department of Physics and Astronomy, McMaster University, Hamilton, Ontario, Canada L8S 4M1.*

¹²*University of Massachusetts, Department of Astronomy, LGRT 619-E, 710 N. Pleasant Street, Amherst, Massachusetts 01003-9305, USA.*

¹³*Department of Physics (Astrophysics Group), H. H. Wills Physics Laboratory, Tyndall Avenue, Bristol BS8 1TL, UK.*

¹⁴*Department of Physics and Astronomy, University of California, Los Angeles, PAB, 430 Portola Plaza, Los Angeles, California 90095-1547, USA.*

¹⁵*Department of Physics and Astronomy, 6224 Agricultural Road, University of British Columbia, Vancouver, British Columbia, Canada V6T 1Z1.*

¹⁶*Department of Physics and Astronomy, University of Leicester, Leicester LE1 7RH, UK.*

¹⁷*Laboratoire Galaxies et 'Etoiles, Physique et Instrumentation, CNRS UMR 8111, Observatoire de Paris, 5 Place Jules Janssen, 92195 Meudon, France.*

In hierarchical cosmological models¹, galaxies grow in mass through the continual accretion of smaller ones. The tidal disruption of these systems is expected to result in loosely bound stars surrounding the galaxy, at distances that reach 10 – 100 times the radius of the central disk^{2,3}. The number, luminosity and morphology of the relics of this process provide significant clues to galaxy formation history⁴, but obtaining a comprehensive survey of these components is difficult because of their intrinsic faintness and vast extent. Here we report a panoramic survey of the Andromeda galaxy (M31). We detect stars and coherent structures that are almost certainly remnants of dwarf galaxies destroyed by the tidal field of M31. An improved census of their surviving counterparts implies that three-quarters of M31’s satellites brighter than $M_V < -6$ await discovery. The brightest companion, Triangulum (M33), is surrounded by a stellar structure that provides persuasive evidence for a recent encounter with M31. This panorama of galaxy structure directly confirms the basic tenets of the hierarchical galaxy formation model and reveals the shared history of M31 and M33 in the unceasing build-up of galaxies.

Precise measurements of stars and star clusters within the Milky Way have contributed significantly to the development of a cosmological model for galaxy formation^{5,6}. The discovery that the Sagittarius dwarf galaxy was being cannibalized by the Milky Way⁷ brought into sharp focus the role of satellite accretion in the build-up of a galaxy’s mass. Models now propose that galaxies form within dark-matter haloes that grow through the continual accretion and merger of smaller sub-haloes. The predicted number of sub-haloes is at least a few orders of magnitude more than the number of dwarf galaxies observed as satellites around the Milky Way^{8,9}. If we assume

that the underlying cosmology is correct, this implies that either significant numbers of satellites remain undiscovered or only a fraction of sub-haloes contain baryons (stars and gas). In either case, the number, luminosity and spatial distributions of satellite galaxies are important but poorly determined quantities whose values depend strongly on the processes through which baryons are accreted and retained by sub-haloes^{10,11}. Many of the luminous sub-haloes are expected to be perturbed, and even shredded, by the tidal field of the host galaxy, leaving behind stellar debris in the form of streams and substructures within a diffuse stellar halo^{2,3}.

Systematic studies of the Milky Way’s stellar halo, such as with the Sloan Digital Sky Survey¹², have recently revealed a large number of dwarf galaxies and tidal streams. However, our viewpoint from within the Milky Way introduces selection effects and difficulties in interpretation, making a homogeneous global study difficult. To this end, we have initiated the “Pan-Andromeda Archaeological Survey” (PAndAS), a programme using the 1-square-degree field-of-view MegaPrime/MegaCam camera on the 3.6 m Canada-France-Hawaii Telescope (CFHT). We are imaging the closest spiral galaxy, M31, and its less massive companion M33. Once completed, the survey will cover more than 300 square degrees (more than 70,000 kpc²) and extend to a maximum projected radius from M31’s centre of $r_p < 150$ kpc. It is the largest contiguous imaging survey of a massive galaxy and spans the stellar halo out to extremely large radii. PAndAS builds on earlier Isaac Newton Telescope and CFHT photometric studies of this galaxy^{13–17}. It surveys in the g (4, 140 – 5, 600 Å) and i (7, 020 – 8, 530 Å) bands and resolves individual stars in M31 to depths of $g = 26.5$, $i = 25.5$ at a signal-to-noise ratio of 10. The programme started in August 2008 and will continue until January 2011.

Figure 1 shows the spatial density distribution of sources in our extant PAndAS fields that are consistent with red giant branch (RGB) stars in M31. Although the region surveyed so far covers ~ 220 square degrees (nearly 100-fold the area of the classical optical disk of M31), we find RGB stars everywhere across our survey. These stars trace the low-luminosity structure of the galaxy and reveal the vast extent of M31, challenging the commonly held impression of the size of this typical bright galaxy (and, by extension, other galaxies of similar luminosities). These stars are unlikely to have formed in situ at these radii because it is improbable that the local density of gas was high enough to promote star formation. Instead, it is expected that the stars have been accreted from dwarf galaxies or proto-galactic fragments, a conclusion that is consistent with the basic tenets of hierarchical galaxy formation.

Our interpretation of halo stars as accreted relics is supported by the presence of multiple, large, coherent substructures over our survey area. Some of these features, such as the giant stellar stream¹³ (no. 5 in Fig. 1), were previously known. New structures discovered in our survey include a radial overdensity along the northwest minor axis extending nearly 100 kpc from M31 (no. 6), a diffuse structure to the southwest coherent over an arc spanning ~ 40 kpc at a distance of ~ 100 kpc from M31 (no. 7), and an apparent continuation of a previously known stream in the east¹⁶, ~ 50 kpc from M31 that loops around to the north of the galaxy (no. 4). The large scale of the new structures is striking, as is their distance from the centre of M31. They are expected to maintain coherence for at least a few gigayears in the inner halo ($r_p < 50$ kpc), and at least a Hubble time in the outer halo ($r_p > 100$ kpc)¹⁸. The implication is that these structures are the remains of previously accreted dwarf galaxies. None of the newly discovered stellar structures

clearly correlate with HI detections in the environs of M31 (ref. 19). Although the lack of young stars tracing sites of star formation implies that high HI column densities are not expected, more detailed predictions on the HI content of these substructures are not yet possible.

The surviving counterparts of the progenitors of these substructures - the dwarf galaxies - are visible in Fig. 1 as concentrated, round, overdensities, and the large area surveyed permits an improved census of these objects. In Fig. 2a we plot the projected radial number density distribution of galaxies around M31; the profile shows no sign of declining within 150 kpc. In Fig. 2b we plot the cumulative luminosity distribution of all galaxies around M31. We find that it is well described by the usual Schechter function²⁰ with a faint-end slope of $\alpha = 0.98 \pm 0.07$, where the uncertainty represents the standard deviation. These distributions imply that 6 ± 4 satellites more luminous than $M_V \approx -6$ still remain to be discovered within 150 kpc (10 degrees) of M31. Extrapolating the observed flat number-density profile outwards then suggests that M31 may have as many as 88 ± 20 such satellites out to $r_p < 300$ kpc (roughly equal to the expected virial radius of M31's dark-matter halo; see Supplementary Information), only about one-quarter of which are currently known. The derived number is an upper limit, because we expect the radial profile to decline beyond the survey area. Thus, even accounting for observational incompleteness, there is still an order of magnitude too few satellites compared with the expected number of dark-matter haloes. If some of these haloes do not contain stars, then a comprehensive inventory of those that do may shed much light on the solution to the “missing satellites problem”.

The brightest of M31's satellite companions, M33, is surrounded by a previously unknown

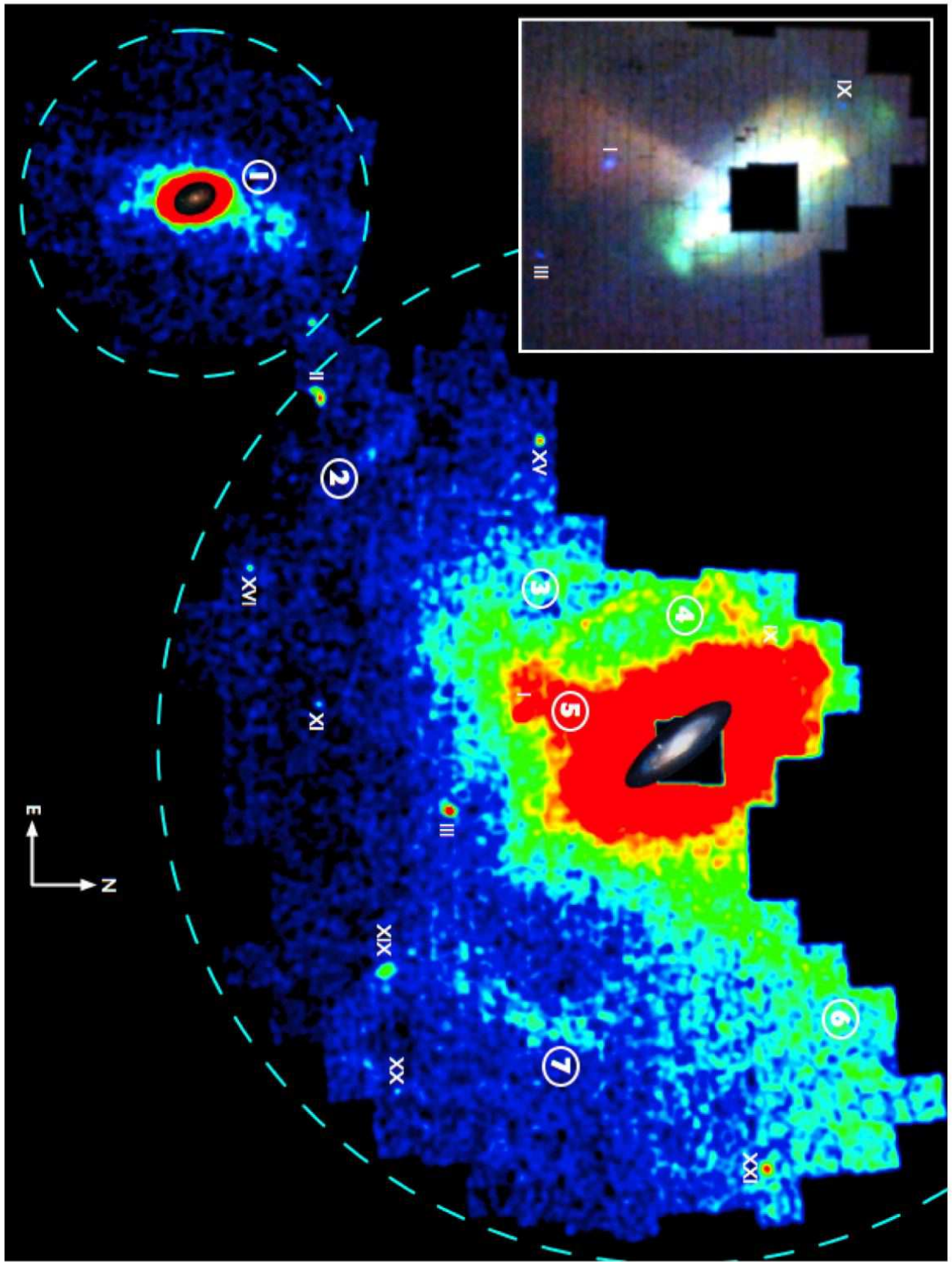
prominent stellar structure (no. 1 in Fig. 1). This feature has an extension stretching ~ 2 degrees (~ 30 kpc projected) to the northwest towards M31, nearly three times farther out than the classical disk of M33. A second extension is also visible in the south. One possible origin of this structure is that it is the accreted remains of a dwarf satellite, similar to the structures observed around M31. However, a long-standing puzzle about M33 is the existence of an extremely warped HI disk, with no apparent counterpart in the “pristine” stellar disk^{21,22}. What process could distort the HI disk but leave the stellar disk unaffected? The newly discovered feature has a similar orientation to the HI warp, suggesting that we have discovered its optical counterpart. Furthermore, the general northwest - southeast symmetry of the distortion, and the broad alignment of the northwest extension with the measured transverse velocity of M33 (ref. 23), are evidence of a tidal disturbance excited as this galaxy orbits around M31.

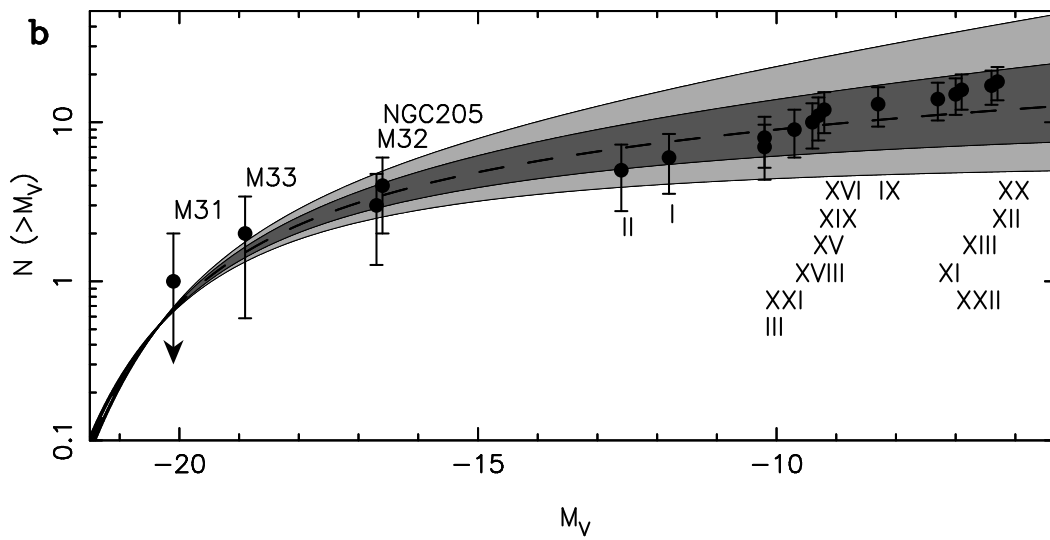
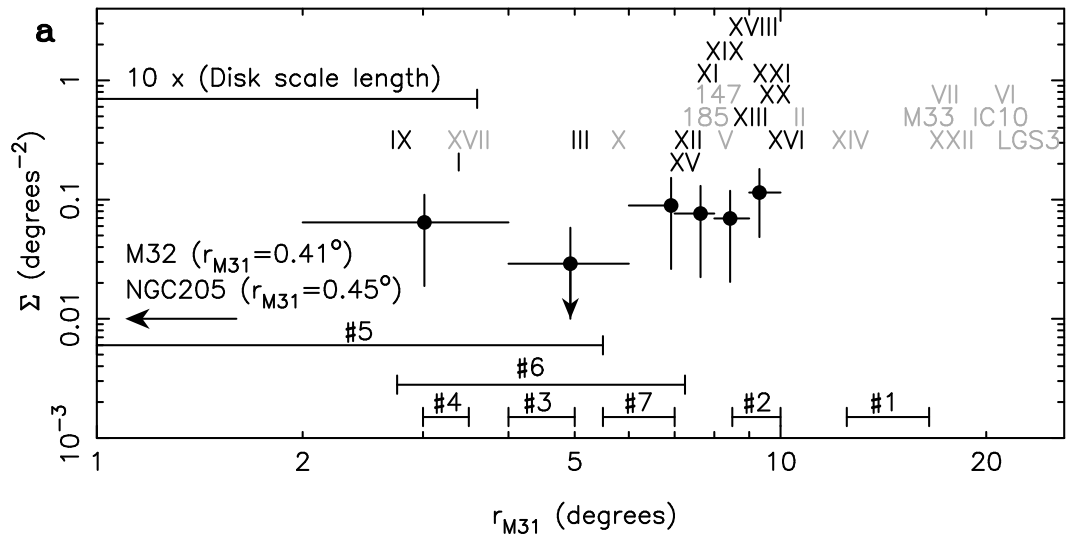
We test this hypothesis by considering the M33 - M31 orbit. If the orbit of M33 carries it close to M31, the tidal field of the latter will excite the M33 disk and eject stars, but the orbit cannot be so close that M33 is severely distorted or disrupted²⁴. We use the techniques described in the Supplementary Information to search for M33 orbits that are consistent with the known constraints and have reasonably close encounters with M31. The search reveals that the smallest possible pericentre distance is ~ 40 kpc, with close passage occurring a few billion years ago. We select several representative orbits and carry out n-body simulations²⁵ of the encounter.

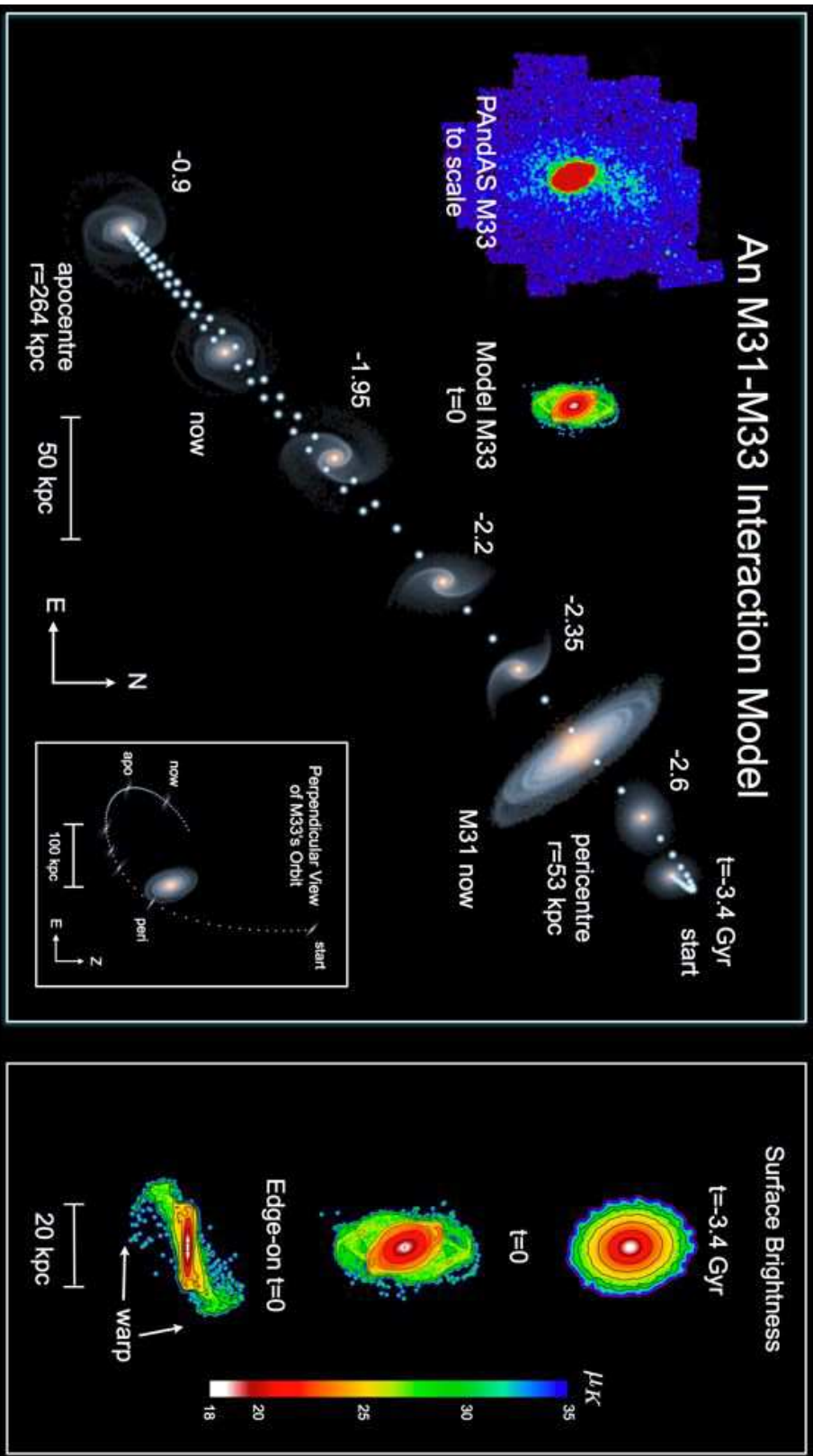
Figure 3 and Supplementary Movie 1 show results from one plausible interaction model. This orbit reproduces with good accuracy the observed distances²⁶, angular positions and radial

velocities of M31 and M33, as well as the proper motion of M33 (ref. 23). The interaction excites tidal tails in the M33 disk that wind up to form an extended distribution of stars with dimensions similar to those of the debris observed in the PAndAS data. In addition, the debris is warped away from the disk in the same sense as the known gaseous warp^{21,22}, lending further support to the interaction hypothesis.

Finally, we note that the encounter between M31 and M33 leaves an imprint on the larger system, exciting a mild warp and disturbances in the M31 disk at large radii. These phenomena are consistent with some of the unusual features observed in the outer regions of M31 (ref. 14), particularly with the discovery of younger stellar populations in these fields²⁷ and with the measured rotational signature shared by many of the substructures²⁸. It is plausible that these stars were originally formed in the thin disk and excited to their present locations by a galactic interaction, perhaps with M33 at an earlier phase in its orbit. The unrivalled panorama of galaxy structure presented here for M31 therefore reveals the continuing role of accretion and interactions in shaping its properties, and is a startling visual demonstration of the truly vast scale of galaxies.







Supplementary Information

1. Galaxy Models

We construct realistic, self-consistent models for M31 and M33 for use in our simulations. They consist of an exponential disk, a Sersic bulge, and a spherical cuspy dark matter halo. From these we construct a self-consistent distribution function and so generate equilibrium N-body systems for simulations. The key structural parameters for the model used in the simulation are given in Supplementary Table 1. The masses of the three components, M_h , M_d , and M_b are given in units of $10^{10} M_\odot$. M33 is naturally truncated by the tidal field of M31 at a radius of ~ 50 kpc at the initial distance of 230 kpc in the model so we quote the M33 halo mass within this tidal radius. Note that for an isolated galaxy with M33's rotation curve, we would normally infer a virial radius > 100 kpc and virial mass about twice that quoted in the table below so it is important to truncate the model in this context. The M31 model extends to a virial radius of $r_{virial} = 280$ kpc and we quote the halo mass inside this radius. The halo scale radius, r_s , the disk scale length, R_d , and the effective radius of the bulge, R_e , are given in kiloparsecs. The Sersic index of the bulge is n_s . We have chosen a suitable mass-to-light ratio for the disk components to ensure that the disks are both intrinsically stable against the formation of a strong bar. To probe the evolution of the outer disks, we truncate the M33 model at 10 scale-lengths (13 kpc) and the M31 model at 7 scale-lengths (40 kpc). These radii are larger than the classical size of the optical disks that extend to approximately 5 scale-lengths.

2. Orbital Model

We set our galaxy models up on a orbit that will lead to an interaction while satisfying the observed constraints. We define the orbit relative to the M31 centre. The assumed distances imply a current separation of M31 and M33 of 206 kpc. We move from heliocentric coordinates to a frame with an origin at the Galactic centre and correct for the effect of Galactic rotation using standard values of the rotation velocity and motion with respect to the Local Standard of Rest. The proper motion of M31 is as yet unmeasured so the transverse velocity components of M31 are unconstrained. However, if we assume values of the M31 proper motion then we can fully determine the current relative position and velocity and so determine the orbit. Finally, the inclination and position angles and direction of rotation of M31 and M33 determine the orientation of their respective disks in space. We assume that relative orientations of the two galaxies remain essentially unchanged during an interaction implying that the initial orientation of the two disks is the same as it is at the current epoch in an orbital model.

We now try to find an orbit (or family of orbits) that satisfy the observed constraints. The main unknowns are the M31 transverse velocity components so we allow these to vary as free parameters. We first search the orbital space by integrating the motion of a M33 test particle in the gravitational potential of the M31 model defined above. Our goal is to find orbits with initial conditions that permit a strong enough tidal encounter to excite the observed features in M33. We therefore search for orbits that have close encounters. In test particle integrations, the observed constraints appear to limit the pericenter distance to a value no smaller than $r_p \approx 40$ kpc. In an effort to excite the strongest response we therefore confined ourselves to orbits with $r_p < 50$ kpc which narrows the range of possible orbits considerably. Most orbits tend to be confined to a plane

nearly parallel to our line of sight and most of the interactions occur with the past few billion years. The model presented in this paper is representative of this family.

Dynamical friction is a further complication. Its effect was significant and affected our predictions of initial conditions based on the test particle integrations above. We therefore incorporate dynamical friction into our orbital search calibrating the parameters in the dynamical friction formula using the N-body simulations. In this way, it was possible to predict initial conditions for the simulations that would result in the M31 and M33 systems ending up in the current positions and relative velocities within the errors of the known constraints and assumed proper motion of M31.

3. N-body Model

We construct N-body models with a total of 6.7 million particles divided up according to Supplementary Table 2. This numerical resolution was adequate to illustrate the main features of a tidal encounter though future work will increase particle numbers to resolve finer details of the interaction. The simulation was carried out using a parallelized tree-code.

4. Uniqueness of the model

The observed constraints on the relative position and velocity of M33 along with the assumption of a close encounter lead to a range of models similar to the one presented in this paper. Another implicit assumption in determination of this orbit is the gravitational potential of M31 with parameters described above. The outer mass profile and virial mass of M31 might be differ-

ent and this would change the detailed character of the orbit and interaction. However, the inner mass profile of M31 is well-constrained so the strength of the tidal encounter will not be significantly different in models where the outer mass profile varies. So while the model presented here is not unique it demonstrates with reasonable accuracy the effect of a recent close encounter on the evolution of M33 in a plausible orbit.

The model demonstrates that such an encounter will excite tidal tails in the outer disk of M33 shortly after the encounter as well as a warp. As the galaxy proceeds along its orbit, these features wind up leaving a disturbed outer disk. The extent of these features will depend in detail on the initial truncation radius of the disk and pericentric separation. Also, the phase of disk extension and warp will depend on the exact timing of the orbit. Matching up all these details simultaneously with all constraints is a difficult challenge, but the model presented here demonstrates quite clearly that a disturbance in the stellar disk and a warp with similar properties to the observed features can be generated by a recent interaction that is sufficiently close.

1. White, S. D. M. & Rees, M. J. Core condensation in heavy halos at two-stage theory for galaxy formation and clustering. *Mon. Not. R. Astron. Soc.* 183, 341-358 (1978).
2. Bullock, J. S. & Johnston, K. V. Tracing galaxy formation with stellar halos. I. Methods. *Astrophys. J.* 635, 931-949 (2005).
3. Abadi, M. G., Navarro, J. F. & Steinmetz, M. Stars beyond galaxies: the origin of extended luminous haloes around galaxies. *Mon. Not. R. Astron. Soc.* 365, 747-758 (2006).
4. Johnston, K. V. et al. Tracing galaxy formation with stellar halos. II. Relating substructure in phase and abundance space to accretion histories. *Astrophys. J.* 689, 936-957 (2008).
5. Eggen, O. J., Lynden-Bell, D. & Sandage, A. R. Evidence from the motions of old stars that the Galaxy collapsed. *Astrophys. J.* 136, 748-766 (1962).
6. Searle, L. & Zinn, R. Compositions of halo clusters and the formation of the galactic halo. *Astrophys. J.* 225, 357-379 (1978).
7. Ibata, R. A., Gilmore, G. & Irwin, M. J. A dwarf satellite galaxy in Sagittarius. *Nature* 370, 194-196 (1994).
8. Klypin, A., Kravtsov, A. V., Valenzuela, O. & Prada, F. Where are the missing galactic satellites? *Astrophys. J.* 522, 82-92 (1999).
9. Moore, B. et al. Dark matter substructure within galactic halos. *Astrophys. J.* 524, L19-L22

(1999).

10. Bullock, J. S., Kravtsov, A. V. & Weinberg, D. H. Reionization and the abundance of galactic satellites. *Astrophys. J.* 539, 517-521 (2000).

11. Kravtsov, A. V., Gnedin, O. Y. & Klypin, A. A. The tumultuous lives of galactic dwarfs and the missing satellites problem. *Astrophys. J.* 609, 482-497 (2004).

12. Belokurov, V. et al. The field of streams: Sagittarius and its siblings. *Astrophys. J.* 642, L137-L140 (2006).

13. Ibata, R., Irwin, M., Lewis, G., Ferguson, A. M. N. & Tanvir, N. A giant stream of metal-rich stars in the halo of the galaxy M31. *Nature* 412, 49-52 (2001).

14. Ferguson, A. M. N., Irwin, M. J., Ibata, R. A., Lewis, G. F. & Tanvir, N. R. Evidence for stellar substructure in the halo and outer disk of M31. *Astron. J.* 124, 1452-1463 (2002).

15. Martin, N. F. et al. Discovery and analysis of three faint dwarf galaxies and a globular cluster in the outer halo of the Andromeda galaxy. *Mon. Not. R. Astron. Soc.* 371, 1983-1991 (2006).

16. Ibata, R. et al. The haunted halos of Andromeda and Triangulum: a panorama of galaxy formation in action. *Astrophys. J.* 671, 1591-1623 (2007).

17. McConnachie, A. W. et al. A trio of new Local Group galaxies with extreme properties. *Astrophys. J.* 688, 1009-1020 (2008).

18. Johnston, K. V., Hernquist, L. & Bolte, M. Fossil signatures of ancient accretion events in the halo. *Astrophys. J.* 465, 278-287 (1996).
19. Thilker, D. A. et al. On the continuing formation of the Andromeda galaxy: detection of HI clouds in the M31 halo. *Astrophys. J.* 601, L39-L42 (2004).
20. Schechter, P. An analytic expression for the luminosity function for galaxies. *Astrophys. J.* 203, 297-306 (1976).
21. Rogstad, D. H., Wright, M. C. H. & Lockhart, I. A. Aperture synthesis of neutral hydrogen in the galaxy M33. *Astrophys. J.* 204, 703-711 (1976).
22. Corbelli, E. & Schneider, S. E. A warped disk model for M33 and the 21 centimeter line width in spiral galaxies. *Astrophys. J.* 479, 244-257 (1997).
23. Brunthaler, A., Reid, M. J., Falcke, H., Greenhill, L. J. & Henkel, C. The Geometric distance and proper motion of the Triangulum Galaxy (M33). *Science* 307, 1440-1443 (2005).
24. Loeb, A., Reid, M. J., Brunthaler, A. & Falcke, H. Constraints on the proper motion of the Andromeda galaxy based on the survival of its satellite M33. *Astrophys. J.* 633, 894-898 (2005).
25. Dubinski, J. A parallel tree code. *N. Astron.* 1, 133-147 (1996).
26. McConnachie, A. W. et al. Distances and metallicities for 17 Local Group galaxies. *Mon. Not. R. Astron. Soc.* 356, 979-997 (2005).

27. Richardson, J. C. et al. The nature and origin of substructure in the outskirts of M31. I. Surveying the stellar content with the Hubble Space Telescope Advanced Camera for Surveys. *Astron. J.* 135, 1998-2012 (2008).
28. Ibata, R. et al. On the accretion origin of a vast extended stellar disk around the Andromeda galaxy. *Astrophys. J.* 634, 287-313 (2005).
29. Dotter, A. et al. The Dartmouth stellar evolution database. *Astrophys. J. Suppl. Ser.* 178, 89-101 (2008).
30. Widrow, L. M., Pym, B. & Dubinski, J. Dynamical blueprints for galaxies. *Astrophys. J.* 679, 1239-1259 (2008).

Acknowledgements We thank the entire staff at the Canada - France - Hawaii Telescope for taking the data, for initial processing with Elixir and for their continuing support throughout this project. A.M.N.F. and A.D.M. are supported by a Marie Curie Excellence Grant from the European Commission under contract MCEXT-CT-2005-025869. G.F.L. thanks the Australian Nuclear Science and Technology Organisation (ANSTO) for supporting his involvement in PAndAS through its Access to Major Research Facilities Program (AMRFP). R.M.R. acknowledges grant AST-0709479 from the National Science Foundation, and grants GO-9453, GO-10265 and GO-10816 from the Space Telescope Science Institute. The image of M33 overlaid in Fig. 1 is reproduced by courtesy of T. A. Rector and M. Hanna.

Competing Interests The authors have no competing financial interests.

Author contributions All authors assisted in the development and writing of the paper. In addition, A.W.M. is the Principal Investigator of PAndAS; M.J.I. led the data processing effort; R.A.I. was the Principal Investigator of an earlier CFHT MegaPrime/MegaCam survey, which PAndAS builds on (which included S.C.C., A.M.N.F., M.J.I., G.F.L., N.F.M., A.W.M. and N.T.); J.D., L.M.W. modelled the M31 - M33 interaction; N.F.M. had a lead role in the study of the dwarf galaxies; P.C. assisted with constructing the luminosity function; and A.L.D. developed the theoretical isochrones.

Correspondence Reprints and permissions information is available at www.nature.com/reprints. Correspondence and requests for materials should be addressed to A.W.M. (alan.mcconnachie@nrc-cnrc.gc.ca).

Figure 1 Stellar density map of Andromeda - Triangulum. A tangent-plane projection of the density distribution of stellar sources in our extant PAndAS imaging is shown, with colours and magnitudes consistent with RGB stars at the distance of M31. The inset shows the central parts of our survey at higher resolution. Dashed circles represent the maximum projected radii of 150 and 50 kpc from M31 and M33, respectively. Scale images of the disks of M31 and M33 are overlaid. Visible dwarf satellites are indicated with roman numerals. Numbers in circles indicate the largest and most obvious substructures detected in a visual inspection of the image: 1, M33 structure; 2, 125-kpc stream (stream A); 3, stream C; 4, eastern arc (stream D); 5, giant stellar stream; 6, northwest minor-axis stream; 7, southwest cloud. Features 1, 6 and 7 (and part of 4) are new discoveries. Stellar sources were identified by using star-galaxy classification techniques described previously^{14,16}. Candidate RGB stars were selected by their position in a colour-magnitude diagram relative to theoretical isochrones²⁹ for a 12-Gyr population at the distance of M31 (ref. 26), using only stellar sources with $i_0 < 23.5$. A projection of the stellar density distribution within a putative metallicity range $-2.5 < [Fe/H] < -0.6$ dex was created with 0.02×0.02 pixels, smoothed with a Gaussian filter with dispersion 3 arcmin, and displayed with square-root scaling. The inset was created by combining, with a red-green-blue colour scheme, three such maps of M31 with metallicities of $-0.4 < [Fe/H] < +0.2$ dex, $-1.3 < [Fe/H] < -0.4$ dex and $-2.3 < [Fe/H] < -1.3$ dex, respectively (each with 0.01×0.01 degree pixels, smoothed with a Gaussian filter with 2 arcmin dispersion) and displayed with logarithmic scaling. Not all structures are visible with this (or any other)

choice of metallicity cut, filter and scaling.

Figure 2 Distribution of M31 dwarf galaxies. **a**, Points show the projected radial number density of dwarfs (Σ), derived for galaxies within 10 degrees of M31 in the survey region. Horizontal error bars show the size of the bin, with points plotted at the mean galaxy radius in that bin. Vertical error bars are Poissonian. Galaxy names in black indicate the positions of the galaxies contributing to each bin; the remaining galaxies are named in grey. The radial ranges of the substructures indicated in Fig. 1 are also shown. **b**, The luminosity distribution, using all galaxies within the survey. Error bars are Poissonian. The dashed line shows the best-fit Schechter function, with slope $\alpha = 0.98 \pm 0.07$. Dark and light grey areas show 1σ and 2σ deviations in α , respectively. In both panels we are probably missing some satellites within ~ 4 degrees of M31, where the high stellar density makes it difficult to detect faint satellites. We can detect galaxies brighter than $M_V < 26$, although derivation of the exact incompleteness levels remains to be calculated for the completed survey. To avoid these selection effects, the slope of the luminosity function is derived by using a χ^2 fit of a Schechter function to galaxies brighter than $M_V < -8$, where incompleteness is not an issue, and we note that the extrapolation to lower luminosities fits these data well. Because of the lack of bright galaxies, we cannot independently derive M^* . Instead, we fix M^* at a range of values and derive corresponding values of α , finding that α is robust to within 1σ for $-19.5 > M^* > -21.5$ (with a trend such that fainter values for M^* correspond to lower values for α). The quoted value of α corresponds to $M^* = -21$.

Figure 3 An M31 - M33 interaction. **a**, The evolution of M33 about M31 along an orbit consistent with the angular positions, distances²⁶ and radial velocities of M31 and M33 and with M33's proper motion²³. Here, M33 starts 3.4 Gyr ago at a distance of $r < 200$ kpc on the far side of M31 falling down the line of sight to the Milky Way. After 800 Myr, M33 reaches pericentre and proceeds across our line of sight towards the southeast, reaching apocentre about 900 Myr ago before falling back towards M31 to its current position. Dots tracing the orbit are separated by 49 Myr to give a sense of the speed along the orbit. The lower inset shows a perpendicular view of M33's orbit. **b**, Quantification of the expected K-band surface brightness of M33 at different times from face-on and edge-on perspectives. The inner red/orange region with $\mu_K < 22$ mag arcsec⁻² defines the size of the usual optical disk of M33 seen in images. The initial equilibrium models³⁰ for the two galaxies consist of a disk, bulge and dark-matter halo with structural parameters that accurately reproduce the observed surface brightness profiles and rotation curves. Because the mass profile of M31 beyond 100 kpc is not well constrained by observations, we appeal to cosmological arguments²⁴ that predict a mass of 2.5×10^{12} solar masses within $r < 280$ kpc. See the Supplementary Information for more details.

	Halo		Disk		Bulge		
	M_h	r_s	M_d	R_d	M_b	R_e	n_s
M33	8	12	0.26	1.3	0.055	0.84	2.5
M31	247	22	5.8	5.8	3.3	1.5	1.0

Table 1: Equilibrium galaxy parameters

	Halo	Disk	Bulge
	N_h	N_d	N_b
M33	2M	1M	200K
M31	2M	1M	500K

Table 2: Numerical resolution